Copy No. 10

NASA Program Apollo Working Paper No. 1108

AN ANALOG SIMULATOR STUDY OF APOLLO ENTRY MONITORING SYSTEMS

NATIONAL AERONAUTICS AND SPACE ADMINISTRATION
MANNED SPACECRAFT CENTER
Houston, Texas

March 20, 1964

NASA Program Apollo Working Paper No. 1108

AN ANALOG SIMULATOR STUDY OF APOLLO ENTRY MONITORING SYSTEMS

Prepared By: William H. Hamby
AST, Flight Dynamics Branch

James A. Lawrence
AST, Flight Dynamics Branch

Darwin E. Crawford
AST, Flight Dynamics Branch

Authorized for Distribution:

for Maxime A. Faget
Assistant Director for Engineering and Development

NATIONAL AERONAUTICS AND SPACE ADMINISTRATION

MANNED SPACECRAFT CENTER

HOUSTON, TEXAS

March 20, 1964

TABLE OF CONTENTS

LIST OF FIGURES

AN ANALOG SIMULATOR STUDY OF APOLLO ENTRY MONITORING SYSTEMS

SUMMARY

The earth entry of the Apollo Command Module was simulated in six degrees-of-freedom, using an analog computer to solve all the required equations and to drive the pilot's displays. To test the pilot's ability to utilize entry monitoring systems, an automatic entry guidance system was programed and then systematically failed to simulate emergency conditions. The pilots utilized two types of flight monitors as aids in detecting failures of the automatic guidance system: (1) an X-Y plotter showing a continuous trace of total acceleration versus total velocity and (2) an instrument showing the difference between the present value of total acceleration and a computed minimum value below which atmospheric "skip" will occur. The present value of total acceleration was shown on a separate instrument. The pilots monitored a series of entries, using each of the two monitoring systems, and took manual control when failures of the automatic system were believed to have occurred. Manual control was effected by means of a three-axis hand controller actuated by the pilot's right hand.

Results of this study indicate that either of the two monitoring systems will provide a satisfactory entry monitoring capability under most anticipated entry conditions.

INTRODUCTION

The primary entry guidance system for the Apollo vehicle will be an automatic, relatively complex system with the capability to handle a wide variety of entry conditions and range requirements (ref. 1). The system will function with some degree of efficiency even in the presence of reasonable errors in the indicated initial position and velocity, initial misalinement of the IMU, errors in the IMU gyros and accelerometers, non-standard atmospheric conditions, and non-standard spacecraft aerodynamic characteristics. However, unexpectedly large errors from a single source or an accumulation of errors from several sources may saturate the system's capability to compensate. In addition, total or partial failures of critical system components (the onboard digital computer, for example) are possible before or during entry. For some types of failure, the system may appear to be functioning normally. For these reasons, it is desirable that an independent and reliable entry monitoring system (EMS) be available to insure a safe entry.

The EMS must be sufficiently accurate to detect impending unacceptable trajectory characteristics in sufficient time to prevent their occurrence; it must not unnecessarily restrict the performance of the primary guidance system; and it must be at least an order of magnitude more reliable than the primary guidance system.

The major survival constraints for Apollo entries are maneuver loads and load histories which exceed crew emergency limits, atmospheric exits at velocities greater than local circular orbit velocity, heating conditions which exceed the thermal design limits, and flight times which exceed vehicle design limits. An EMS designed to avoid these constraints and to permit effective monitoring of the primary guidance system is currently envisioned as consisting of four basic parts: an entry threshold indicator, a corridor indicator, a bank attitude indicator, and a flight monitor.

The entry threshold indicator is an on-off signal that is excited when the sensed acceleration is greater than some nominal value. The corridor indicator consists of two signals used to indicate whether the entry is in the top or bottom of the entry corridor. The signals result from comparing the sensed acceleration to a nominal mid-corridor value at a discrete time interval after the threshold indication. The bank attitude indicator is a meter indicating angular rotation about the approximate stability axis (X_S). The necessity of the threshold and corridor indicators is debatable since the pilot can obtain the needed information directly from accelerometer readings. These two indicators were not mechanized for the present simulator, and no difficulties ensued as a result of their omission. However, these indicators can be included in the Apollo vehicle with little difficulty, and the resulting reduction of the pilot's tasks may make them worthwhile. The bank attitude indicator and the flight monitor are essential to a workable EMS.

A simulator study of two possible EMS displays was conducted by the Flight Dynamics Branch of the Spacecraft Technology Division. The purpose of this study was to determine the general requirements of the entry monitoring problem, and to compare the effectiveness of the two EMS displays now under consideration for the Apollo vehicle.

SYMBOLS

General

a	Resultant aerodynamic acceleration
a_r	Reference value of a
$C_{1,2,3}$	Capacitors
C_A	Axial force coefficient
C_N	Normal force coefficient
C_m	Static moment coefficient
C_{m_q}, C_{l_p}	Damping coefficients
D	Reference vehicle diameter; also drag acceleration (lbs)
G	Resultant aerodynamic acceleration; also drag acceleration (g's)
g	Acceleration due to the central force-field gravity component at altitude h
g_o	Acceleration due to the central force-field gravity component at sea level
G_s	Acceleration below which uncontrolled atmospheric skip will occur
h	Altitude
h_o	Reference altitude
$\dot{h}$	Altitude rate
$\dot{h}_b$	Bias in measured value of $\dot{h}$
$\dot{h}_r$	Reference $\dot{h}$

I_x, I_y, I_z	Moments of inertia
I_{xz}	Product of inertia
K_1	Reference value of L/D in guidance system
$K_{1,2}$	Arbitrary constants in G-G_s flight monitor
$K_{2,3,4}$	Linear gains in guidance system
K_5	Total range of reference trajectory
$k_{A,h}$	Weighting factors
L	Latitude
L_T	Latitude of target
L_b, M_b, N_b	Body axes moments
L/D	Lift to drag ratio
L/D_C	Commanded L/D
L/D_{max}	Maximum value of L/D_C
m	Mass
M	Mach number
M_{jx}, M_{jy}, M_{jz}	Control system moments about body axes
$\overline{P}$, $\overline{Q}$, $\overline{R}$	Components of the vehicle angular velocity with respect to the F-Frame along $\overline{i_b}$, $\overline{j_b}$, $\overline{k_b}$, respectively
P_b, Q_b, R_b	Components of the vehicle angular velocity with respect to inertial space along $\overline{i_b}$, $\overline{j_b}$, $\overline{k_b}$, respectively
P_h	Angular velocity of the earth

$\bar{q}$	Dynamic pressure
r	Radial distance from center of earth
r_o	Reference value of r
R_E	Earth radius
S	Reference vehicle area
s	LaPlacian operator
t	Time
t_o	Reference time
U_{a_b}, V_{a_b}, W_{a_b}	Components of relative velocity along $\bar{i}_b$, $\bar{j}_b$, $\bar{k}_b$, respectively
U_{a_f}, V_{a_f}, W_{a_f}	Components of relative velocity along $\bar{i}_f$, $\bar{j}_f$, $\bar{k}_f$
U_e, V_e, W_e	Components of inertial velocity along $\bar{i}_e$, $\bar{j}_e$, $\bar{k}_e$, respectively
U_h, V_h, W_h	Components of inertial velocity along $\bar{i}_h$, $\bar{j}_h$, $\bar{k}_h$, respectively
U_{h_o}	Reference value of U_h
V_A	Resultant relative velocity
V_E	Exit velocity
V_I, V	Resultant inertial velocity
V_o	Initial value of inertial velocity
W_x, W_y	Components of wind velocity along $\bar{i}_e$, $\bar{j}_e$

X_b, Y_b, Z_b	Components of aerodynamic force along $\overline{i}_b$, $\overline{j}_b$, $\overline{k}_b$, respectively
X_f, Y_f, Z_f	Components of aerodynamic force along $\overline{i}_f$, $\overline{j}_f$, $\overline{k}_f$, respectively
X_h, Y_h, Z_h	Components of aerodynamic force along $\overline{i}_h$, $\overline{j}_h$, $\overline{k}_h$, respectively
X_{r_T}	Reference range traversed
X_T	Downrange to go
Y_T	Crossrange to go
Z_i	Input impedance
Z_f	Feedback impedance
α_T	Trim angle of attack
γ	Flight-path angle
Γ_i, Ψ_{h_i}	Angles which orient the F-Frame with respect to the E-Frame [(order of rotation Ψ_{h_i}, Γ_i, o)]
Γ_i, $(\Psi_{h_i}-\Psi_h)$	Angles which orient the F-Frame with respect to the H-Frame [order of rotation $(\Psi_{h_i}-\Psi_h)$, Γ_i, o]
δ_h	Deviation of h from h_o ($\delta_h = h-h_o$)
δ_r	Deviation of r from r_o ($\delta_r = r-r_o$)
δU_h	Deviation of U_h from U_{h_o} ($\delta U_h = U_h-U_{h_o}$)
ϵ_z	Center of gravity offset along $\overline{k}_b$

η	Total angle of attack
λ	Longitude
λ_T	Longitude of target
ρ	Atmospheric density
σ_x	Center of gravity offset measured toward heat shield from aerodynamic reference c.g.
τ	Dummy variable
$\tau_{1,2}$	Time constants
Ψ, θ, ϕ	Euler angles which orient the B-Frame with respect to the F-Frame (order of rotation θ, Ψ, ϕ)
Ψ_h	Azimuth angle
ϕ_b	Aerodynamic resolution angle
ϕ_c	Command bank angle
ω_{x_f}, ω_{y_f}, ω_{z_f}	Components of the angular velocity of the F-Frame with respect to inertial space along $\bar{i}_f$, $\bar{j}_f$, $\bar{k}_f$, respectively

Definition of Direction Cosines

$a_{1,2,3}$	The projection of $\bar{i}_f$, $\bar{j}_f$, $\bar{k}_f$, respectively, onto the x_h axis
$b_{1,2,3}$	The projection of $\bar{i}_f$, $\bar{j}_f$, $\bar{k}_f$, respectively, onto the y_h axis
$c_{1,2,3}$	The projection of $\bar{i}_f$, $\bar{j}_f$, $\bar{k}_f$, respectively, onto the z_h axis
$d_{1,2,3}$	The projection of $\bar{i}_e$, $\bar{j}_e$, $\bar{k}_e$, respectively, onto the x_f axis

$e_{1,2,3}$ The projection of $\overline{i_e}$, $\overline{j_e}$, $\overline{k_e}$, respectively, onto the y_f axis

$f_{1,2,3}$ The projection of $\overline{i_e}$, $\overline{j_e}$, $\overline{k_e}$, respectively, onto the z_f axis

$l_{1,2,3}$ The projection of $\overline{i_b}$, $\overline{j_b}$, $\overline{k_b}$, respectively, onto the x_f axis

$m_{1,2,3}$ The projection of $\overline{i_b}$, $\overline{j_b}$, $\overline{k_b}$, respectively, onto the y_f axis

$n_{1,2,3}$ The projection of $\overline{i_b}$, $\overline{j_b}$, $\overline{k_b}$, respectively, onto the z_f axis

Axis Systems

I-Frame The origin of the I-Frame is the center of the earth. The unit vectors in the I-Frame are $\overline{i_I}$ (along the earth's spin axes, toward the North pole), $\overline{j_I}$ (in the equatorial plane toward a reference position of the Greenwich meridian) and $\overline{k_I}$ (also in the equatorial plane).

N-Frame The N-Frame is identical with the I-Frame except that it rotates with the earth. Unit vectors are $\overline{i_N}$, $\overline{j_N}$, $\overline{k_N}$.

E-Frame The origin of the E-Frame is at the center of gravity of the vehicle. The unit vectors in the E-Frame are $\overline{i_E}$ (North), $\overline{j_E}$ (East), and $\overline{k_E}$ (downward toward the center of the earth).

F-Frame The origin of the F-Frame is at the center of gravity of the vehicle. The F-Frame is oriented with the E-Frame by the constant angles Γ_i and Ψ_{H_i}. Unit vectors are $\overline{i_f}$, $\overline{j_f}$, $\overline{k_f}$.

H-Frame — The origin of the H-Frame is at the center of gravity of the vehicle. The H-Frame is oriented with the E-Frame by the heading angle Ψ_H and with the F-Frame by the angles $(\Psi_{H_i} - \Psi_H)$ and Γ_i. The unit vectors are $\overline{i}_h$ (tangential to the local horizon, in the direction of the inertial velocity V_I), $\overline{j}_H$ (tangential to the local horizon), and $\overline{k}_h$ (toward the center of the earth). Note that $\overline{k}_h \equiv \overline{k}_E$.

B-Frame — The origin of the B-Frame is at the center of gravity of the vehicle. Unit vectors are $\overline{i}_b$ (parallel to the vehicle axes of external symmetry, positive forward), $\overline{j}_b$ (to the right), and $\overline{k}_b$ (toward the "bottom" of the vehicle). The B-Frame is oriented with the F-Frame by the Euler angles θ, Ψ, ϕ.

S-Frame — The origin of the S-Frame is at the center of gravity of the vehicle. The S-Frame is oriented with the B-Frame by the trim angle α_T. Unit vectors are $\overline{i}_s$, $\overline{j}_s$, $\overline{k}_s$.

ENTRY MONITORING SYSTEMS

G-V Flight Monitor

The first flight monitor considered in this study consists of a rectilinear plot of total acceleration versus an initial velocity minus the time integral of the sensed flight-path acceleration:

$$\left(V_o - \int_o^t (D/m)\, d\tau \right)$$

This plot, which is displayed to the pilot, provides both maneuvering and monitoring information. A schematic of the display is shown in figure 1.

The flight trace of G-V is interpreted by the pilot with the aid of criteria etched on the face of the instrument. Two criteria must be met to achieve a safe entry. For every G and V where V is greater than

V_E there exists a limiting dG/dV at which safe atmospheric exits can be made. It can be shown that if the flight trace slope is compared to a set of rays eminating from approximately zero G and an exit velocity V_E (which is less than local circular orbit velocity), a safe exit dG/dV can be defined by tangency of the actual flight trace and the rays. This tangency criterion is in fact conservative, possibly to a prohibitive extent, in some regions of the G-V plane.

Criteria similar to that used for exit monitoring can be applied to avoid excessive acceleration. These criteria take the form of a family of G-limit curves as shown in figure 1. Potential to exceed the high-G boundary exists throughout the entry velocity regime. Consequently, a velocity reset capability must be included in the onboard X-Y plotter to provide the G-V slope throughout entry. A thoroughly experienced pilot might well do an excellent job of avoiding high accelerations with only an accelerometer reading; however, use of the G-V display simplifies the task considerably.

G-G_s Flight Monitor

The second flight monitor, as mechanized for this simulation, does in fact rely on the pilot's ability to monitor for high accelerations with no aids other than an accelerometer. This flight monitor consists of two instruments: (1) an accelerometer and (2) a somewhat similar instrument which displays the difference between the actual total acceleration and an approximate acceleration level below which an unsafe atmospheric exit will occur. This second meter will be referred to as the "G-G_s" meter.

The G-G_s flight monitor is based upon essentially the same principle as the G-V display insofar as atmospheric exit monitoring is concerned. The rays on the G-V display face represent constant derivatives of acceleration with respect to velocity. They simply define the maximum rate, with respect to velocity, at which acceleration can be safely decreased. A somewhat similar criterion can be established utilizing a time derivative of acceleration and a velocity increment term equivalent to one of the rays in the G-V plane. Consider an expression of the form:

$$G_s = K_1 \left[\left(V_o - \int_o^t \frac{D}{M} \, d\tau \right) - V_E \right] - K_2 \frac{dG}{dt}$$

where K_1 and K_2 are appropriate constants. In the G-V plane, the first term in the preceding expression is simply a straight line, or ray, passing through the points $K_1 (V_o - V_E)$, V_o and 0, V_E. The second term is a constant multiplied by the time derivative of acceleration. At the entry threshold, G_s is a positive number approximately equal to $K_1 (V_o - V_E)$. If G_s is considered to be the value of G below which uncontrolled atmospheric skip will occur, this would indicate an emergency situation and require full negative lift, regardless of the entry flight-path angle. As the atmosphere is encountered, the term $K_2 \frac{dG}{dt}$ increases, G increases, V decreases; hence $G-G_s$ increases. When $G-G_s$ becomes positive, a safe atmospheric capture is presumed to have occurred and either positive or negative lift may be used, insofar as unsafe atmospheric skips are concerned. The exit monitoring criterion now requires that $G-G_s$ remain positive for the remainder of the entry. It is apparent that in principle this criterion is just another way of limiting the rate at which the sensible atmosphere is exited. This flight monitor is designed for exit monitoring only; the "skip" indication at the entry interface may be ignored if an atmospheric penetration with full positive lift is desired. Once in the atmosphere, with either positive or negative lift, $G-G_s$ tends to increase until pull-up begins. The rate of increase is proportional to the initial entry flight-path angle and the direction of lift.

Some further insight into the physical meaning of the expression for G_s can be gained by noting that $\frac{dG}{dt} \approx g_o \, G \frac{dG}{dV}$. This also emphasizes the similarity of the manner in which the G-V and the $G-G_s$ flight monitors operate. The functioning of the $G-G_s$ flight monitor depends upon the proper selection of the gains K_1 and K_2 and the exit velocity V_E. Many combinations will work quite well. The values selected for the present study were $K_1 = 0.45 \times 10^{-3}$ sec/ft, $K_2 = 10.0$ sec, $V_E = 25{,}000$ ft/sec. These values yielded excellent results, but are not necessarily optimum. Using these numbers, and assuming no errors, a zero value of $G-G_s$ at atmospheric exit results in a range of about 5,000 nautical miles. In the presence of velocity errors, and a 5,000 nautical mile range requirement, it would be necessary to slightly increase the value of V_E to minimize the chances of incorrectly taking manual control when the primary guidance system is operating normally.

DESCRIPTION OF SIMULATOR

General Characteristics

The simulation of the earth entry of the Apollo Command Module was accomplished by coupling an analog computer mechanization of the equations of motion and the entry guidance equations to a cockpit containing instrument displays and a control actuator. Depending on the mode of operation desired, the pilot could elect to: (1) monitor the entry with the guidance and control systems operating automatically; (2) operate the Reaction Control System (RCS) manually by means of a three-axis hand controller, but utilize the commanded roll angle as generated by the automatic guidance system; (3) take complete manual control on the basis of his interpretation of the EMS display(s).

The ARDC 1959 Standard Atmosphere was used. Static aerodynamic coefficients were obtained from reference 2. Variation of these coefficients with Mach number were ignored. Dynamic aerodynamic coefficients were assumed to be negligibly small. The mass and inertia characteristics of the simulated vehicle are given in table 1. These characteristics were assumed to be constant.

Equations of Motion

A block diagram of the equations of motion utilized is shown in figure 2. These equations are similar to those derived in reference 3. The significant differences are: (1) an axis system (the "F-Frame") was added to provide more flexiblity in initial conditions; (2) the order of rotation of the Euler angles was changed to coincide with the sequence used by the Apollo IMU.

Guidance Equations

The entry guidance system utilized was based on the techniques developed in reference 4. This system was selected because of the relatively small amount of computing equipment required for its mechanization. The Apollo entry guidance system (ref. 1), in its present form, is prohibitively complicated for programing on the limited amount of computing equipment available for this portion of the simulator. A listing of the guidance equations used in this simulation is contained in appendix B.

Flight Monitor Mechanization

The actual onboard mechanization of the G-V Flight Monitor is simple in concept, though possibly difficult in execution. Basically,

the requirements would include an accelerometer, an integrator, and a servo-driven X-Y plotter. Mechanization of this monitor for the simulator used in this study was a simple matter since all the required quantities were directly available.

The mechanization of the $G-G_s$ flight monitor is less straightforward but the requirement for display space is considerably less. Weight and power requirements may also be less on the actual vehicle. In the development of a network to generate the quantity $G-G_s$, it is convenient to temporarily define G to be the drag component of acceleration rather than the total acceleration. So doing, note that the expression $G-G_s$ now involves the drag acceleration, its time integral, and its time derivative. The pilot's display of $G-G_s$ must be reasonably steady. Hypothesizing that a second-order filter is both necessary and sufficient to eliminate the noise in the accelerometer output and time derivative of the accelerometer output, a transfer function of the following form is suggested:

$$\frac{E_o(s)}{E_i(s)} = \frac{g_o \dfrac{K_1}{S} + K_2 S + 1}{(\tau_1 S + 1)(\tau_2 S + 1)} = \frac{g_o K_1 + K_2 S^2 + S}{S(\tau_1 S + 1)(\tau_2 S + 1)} \qquad (1)$$

This transfer function can be mechanized in several ways. Perhaps the most attractive method involves the use of a high gain amplifier with passive elements for input and feedback impedances. Appendix A contains a discussion of the mechanization of 1 used in this study.

Control System

During the atmospheric entry phase of the Apollo mission, the command module control system has three functions to perform. The first of these functions is an exo-atmospheric attitude hold. Prior to entry into the sensible atmosphere, the vehicle must be placed in the proper attitude and held there until aerodynamic acceleration reaches a value of about 0.05 g's. Attitude hold will also be required for longrange trajectories where controlled atmospheric skip is needed. The second control system function is to provide a roll capability within the sensible atmosphere; the third is to damp oscillatory transients in the vehicle's angular motions. The control system must be capable of operation in four modes: attitude hold, automatic position-command in roll with automatic rate damping in pitch and yaw, manual rate-command, and manual acceleration-command.

The control system has two independent sets of constant-thrust reaction jets producing a thrust of approximately 100 pounds each, mounted to produce torques approximately in body axes. The control system is designed so that either of the sets of jets can perform all the required control functions independently, but in the normal operational mode both systems are used simultaneously.

Atmospheric roll maneuvers must be performed in the S-Frame (about $\bar{i}_s$), while the jets are mounted approximately in the B-Frame. Angular rates are also measured in the B-Frame. Coordinated maneuvers about $\bar{i}_s$ accordingly require rate signal-mixing, and also result in large cross-coupling torques. Reference 5 contains a detailed description of the Apollo control systems.

Cross-coupling torques and the necessary rate crossfeeds were accounted for in the simulated control system. Transport lags, delays in thrust buildup and decay, and other system characteristics with relatively small effects on performance, were ignored.

In the automatic mode, angular rates were limited to 17 deg/sec. In the manual rate-command mode, angular rates were limited to about 50 deg/sec. Rates were not limited in the acceleration-command mode, except by the pilot. In all modes except acceleration-command, automatic rate damping was employed, with deadbands of 2 deg/sec. Position-command deadbands of 10° were used in the automatic modes.

Displays and Controller

The pilot's cockpit is pictured in figure 3. Figure 4 is a closeup of the primary instrument display, excluding the X-Y plotter. The displays, and the hand controller, provide only a functional simulation of the Apollo entry. No attempt was made to actually duplicate the Apollo instrumentation, but rather to duplicate, as nearly as possible with the available instruments, the functions of the actual display. The dual-needle meter showing ϕ and ϕ_c is not now a part of the Apollo display (only ϕ is displayed), but a similar instrument is under consideration.

STUDY PROCEDURES

Four pilots were used as primary subjects for this study. All were military or NASA pilots with experience in piloting high-performance aircraft and in serving as subjects in simulation studies. Each of the pilots was asked to monitor a series of guided Apollo entries using the

two flight monitors first simultaneously, then separately. Altitude rate errors were inserted randomly into the primary guidance system, without the pilot's knowledge. The primary objective was to determine whether the pilots could detect failures in time to prevent excessive ranges and/or accelerations. Also of considerable interest was a determination of how well the pilots could distinguish between normal entries and those for which errors of various magnitudes were present. In addition, the effectiveness of the two flight monitors as compared to each other was desired. In this study, the maximum angular rates available to the pilots in the manual rate-command mode were about 50 deg/sec, rather than the 17 deg/sec available in the Apollo Command Module. The available rates in the rate-command mode in the Apollo vehicle are limited to 17 deg/sec because of the characteristics of the SCS rate gyros. If the pilot deflects the hand-controller past this limiting value, the control system operates in the acceleration-command mode. The necessity for this limiting rate is unfortunate, since in a genuine emergency the speed with which the first manual maneuver is made can mean the difference between life and death. The vehicle can be efficiently controlled in the acceleration-command mode, but it is a considerably more difficult control task. The simulator used for this study required that the pilot flip a switch (with his left hand) to change control system modes (fig. 4), rather than deflecting the hand controller past a detent. All of the pilots were asked to control a few entries using only the manual acceleration-command control mode, and none had any particular difficulty in doing so. However, for most of the entries, the pilots were permitted to utilize the rate-command mode exclusively; hence the necessity for the available rates of 50 deg/sec, rather than 17 deg/sec.

After manual take-over, the nominal procedure (as now planned for Apollo) was to attempt to fly a constant acceleration of about 3 to 5 g's. However, the pilots were permitted to utilize the flight monitors for range control if they wished once control of the entry was firmly re-established.

All entries were initiated at an altitude of 400,000 feet and a velocity of 36,000 feet/seconds. Initial flight-path angles of -5.0, -6.0, -6.5, -7.0, -7.2, and -7.4 degrees were used. The desired landing site was considered to be 5,000 nautical miles downrange of the entry point and 200 nautical miles to the left of the initial plane of flight. Several shorter ranges were also flown, but the 5,000 nautical mile range requirement was used in over 90 percent of the simulated entries. Altitude rate errors of -1,000, -500, -200, -100, -50, 0, 50, 100, 200, 500, and 1,000 feet/second, were programed in the primary guidance system, although all of the pilots did not fly all possible combinations of flight-path angles and altitude rate errors.

DISCUSSION OF STUDY RESULTS

General

It is recognized that many different types of entry system failures are possible. However, a complete failure analysis was considered to be beyond the scope of the present study. This study did establish that the pilots could detect impending unacceptable entry trajectory characteristics using either of the two flight monitors. While only one type of failure was investigated (altitude rate errors), the results of the study should apply equally well to many other types of failure since the only failure indications available to the pilots were the characteristics of the entries.

Comparison of the Utility of the Two Flight Monitors

Approximately 400 runs were made during the investigation, divided about equally between the G-V and the G-G_s flight monitors. About 200 of these runs were utilized to familiarize the pilots with the flight monitors, the simulator in general, and the basic problems involved in entry monitoring. It was quickly established that all of the pilots had more difficulty in monitoring the steeper entries; consequently the steeper entries were repeated more often than the relatively easily-monitored shallow and mid-corridor entries. The rapid changes in acceleration and velocity, and the necessity for exiting the sensible atmosphere at steeper angles (to obtain long ranges), are the principal reasons why the steep entries are more difficult to monitor. Another factor which must ultimately be considered is that the steep entries inherently involve high accelerations, possibly detrimental to pilot efficiency.

After the familiarization runs were completed, the pilots were able to avoid ranges greater than about 6,000 nautical miles, and accelerations greater than 10 g's, for all combinations of initial flight-path angles and altitude rate errors utilized in this study. In attempting to use the flight monitors for range control, the pilot sometimes exceeded 6,000 nautical miles range, but in all such cases the guidance system failure had been detected in adequate time to prevent this if their procedure had been to fly a constant-g profile after manual take-over. The greatest range reached in any case was about 7,500 nautical miles. It is emphasized that use of the Apollo EMS for range control is not presently planned; nevertheless, an emergency range-control capability is considered to be highly desirable, and the results of this study indicate that range control may be feasible with either of the two flight monitors.

Using the G-V flight monitor, all of the pilots tended initially to take manual control of all 5,000 nautical mile entries regardless of whether a primary guidance system failure had been programed. This was determined to be a result of the invalidity of the "tangency to a ray" criterion in all regions of the G-V plane except near the origin of the rays. Unless the primary guidance system is specially adapted to fly straight rays in the G-V plane, the tangency criterion can be violated during the course of perfectly normal entries. This feature of the G-V monitor was not unexpected; however, no modification of the primary guidance system was attempted. Instead, the pilots were instructed to use the tangency criterion only as a rough guide, and to delay manual takeover until in their opinion a genuine survival situation was present. This proved to be a satisfactory procedure for the purposes of this study.

A G-V trace, to atmospheric exit, of a normal 5,000 nautical mile entry from an initial flight-path angle of -7.4° is shown in figure 5. Note that the tangency criterion is definitely violated at about 7 g's. Figure 6 shows a G-V trace of the same type of entry with a failure programed in the primary guidance system. The failure, which would have resulted in a range in excess of 8,000 miles, was detected by the pilot in adequate time to accomplish a safe manually controlled atmospheric exit. The point at which the pilot took manual control is indicated. For this particular simulated entry, the pilot had available both the G-V and G-G_s flight monitors. However, neither of the flight monitors actually indicated a survival situation (remembering that the tangency criterion is not utilized directly) at the time at which the pilot took control, and in fact take-over could have been delayed several more seconds. This serves to emphasize a very important aspect of entry monitoring. The pilot had learned what to expect from the primary guidance system as normal entries progressed. In this case, the pilot knew that to avoid overshooting the desired 5,000 nautical mile range, the guidance system should have commanded a bank angle ϕ_c of about 180° at some point after peak g was reached. Instead, the bank angle had never become more than about 90°. The pilot delayed manual take-over until he was sure a failure was present, but did not wait until a survival situation actually existed. This entry and others very similar to it, with and without guidance failures, were repeated many times, using the G-V and G-G_s flight monitors both simultaneously and separately. Essentially identical results were obtained. The ability of the pilots to anticipate survival situations, based upon their knowledge of entry characteristics and the rate of change of their flight monitor indication, proved to be a valuable asset.

The G-V Flight Monitor was found to be very effective in monitoring for excessive accelerations. The G-G_s monitor, as mechanized for this

study, did not provide a direct capability for predicting excessive accelerations. The pilots were able to do a fairly effective job of high-g monitoring with only the accelerometer reading, but considered this to be a distinctly undesirable procedure.

For exit monitoring, the pilots found that it was considerably easier to read the G-G_s monitor than to interpret the meaning of the G-V trace, particularly since the tangency criterion intended for use with the G-V monitor could not be directly utilized.

Use of the ϕ and ϕ_c Meter

The present Apollo display does not include a ϕ_c meter. The pilots found the ϕ_c meter used in this simulation to be very useful. The ϕ_c meter had three attractive features: (1) ϕ_c leads the actual bank angle ϕ, indicating that a maneuver is forthcoming before any change in ϕ occurs; (2) observing the changes in ϕ_c helps the pilots develop a "feel" for entry; (3) failure of ϕ to properly follow ϕ_c provides a rapid indication of control system failure.

CONCLUDING REMARKS

Results of this simulator study of the G-V and G-G_s entry monitoring systems indicate:

1. Excessive ranges can be prevented with little difficulty using either the G-V or G-G_s flight monitors.

2. The G-V flight monitor is effective in monitoring for excessive acceleration. Further study is recommended to determine if a similar capability can be developed for use with the G-G_s flight monitor.

3. A meter showing the value of the commanded bank angle ϕ_c, in addition to the actual bank angle ϕ, is helpful but not essential with either flight monitor.

4. The invalidity of the tangency criterion does not, except in a very minor way, detract from the effectiveness of the G-V flight monitor. It does mean that the invalidity must be acknowledged and compensated for in some manner. Several possible methods of minimizing the effects of the invalidity exist:

a. A thorough pilot training program will permit utilization of the tangency criterion as an aid in detecting failures, but not as a rigid rule which must never be violated.

b. The straight-line rays could be replaced with more nearly exact curved rays.

c. The primary guidance system could be forced to fly straightline rays for normal entries.

The alternate methods (b) and (c) listed above should yield equally good results, although the implementation of either poses some problems. Alternate (c), in particular, has a drastic effect upon the manner in which the primary guidance system operates. A combination of (a), (b), and (c) may be the best approach to the problem.

REFERENCES

1. Lickly, D. J., and Morth, H. R.: Apollo Reentry Guidance. MIT Instrumentation Laboratory, 1963.

2. Moseley, William C., Jr.: NASA Project Apollo Working Paper No. 1022. STG, Langley Field, Va., 1961. (CONFIDENTIAL)

3. Fogarty, L. E., and Howe, R. M.: Flight Simulation of Orbital and Reentry Vehicles. The University of Michigan, 1961.

4. Lessing, H. C., et al: Lunar Landing and Long-Range Earth Reentry Guidance by Application of Pertubation Theory. Paper presented at the Second Manned Space Flight Symposium, Dallas, Texas, 1963.

5. Lum, B. T. F.: Apollo Stabilization and Control System Analysis Manual. North American Aviation, Inc., 1963. (CONFIDENTIAL)

APPENDIX A

The transfer function required for the G-G_s flight monitor can be mechanized in several ways. A circuit which uses a small amount of equipment is of the following form:

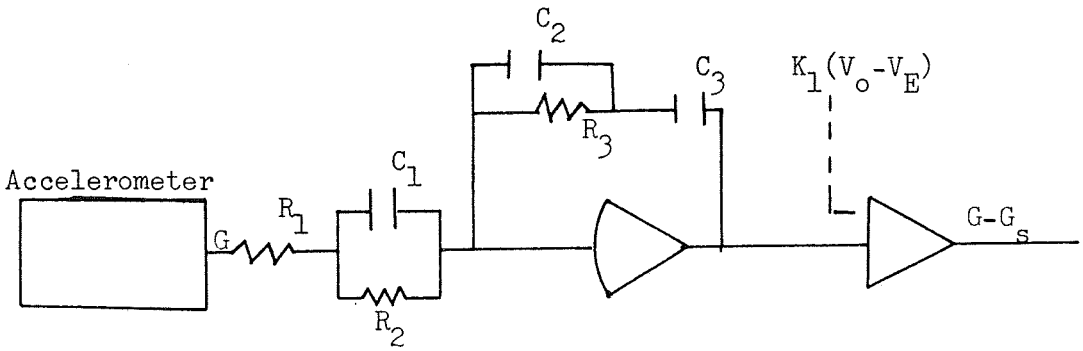

Technically, the constant term $K_1 (V_o - V_E)$ is not a part of the transfer function; however, it is required in the generation of G-G_s and is included to illustrate the form of the complete circuit. Note that the input impedance of the high gain amplifier can be expressed as:

$$Z_i = \frac{(R_1 + R_2)\left[S\left(\frac{C_1 R_1 R_2}{R_1 + R_2}\right) + 1\right]}{SC_1 R_2 + 1}$$

and that the amplifier feedback impedance is:

$$Z_f = \frac{SC_2R_3 + SC_3R_3 + 1}{SC_3\left(SC_2R_3 + 1\right)}$$

The resulting transfer function for the high gain amplifier is:

$$\frac{E_o(s)}{E_i(s)} = \frac{S^2C_1R_2\left[C_2R_3 + C_3R_3\right] + S\left[C_1R_2 + C_2R_3 + C_3R_3\right] + 1}{SC_3\left(R_2 + R_1\right)\left[SC_2R_3 + 1\right]\left[S\left(\frac{C_1R_1R_2}{R_1 + R_2}\right) + 1\right]}$$

Comparing this with the required transfer function given in (1), it is seen that (among other possibilities):

$$K_2 = \frac{C_1R_2\left(C_2R_3 + C_3R_3\right)}{C_3\left(R_1 + R_2\right)}$$

$$1 = \frac{C_1R_2 + C_2R_3 + C_3R_3}{C_3\left(R_1 + R_2\right)}$$

$$g_oK_1 = \frac{1}{C_3\ R_2 + R_1}$$

$$\tau_1 = C_2R_3$$

$$\tau_2 = \frac{C_1R_1R_2}{R_1 + R_2}$$

As previously indicated, $K_1 = 0.45 \times 10^{-3}$ and $K_2 = 10$. Satisfactory (but not necessarily optimum) values of the time constants are $\tau_1 = 1.0$ and $\tau_2 = 1.0$. There remain six unknowns, and only five equations to satisfy. One of the unknowns may be arbitrarily chosen. Assuming, for instance, that $R_2 = 10$ m Ω, the remaining unknowns are: $R_1 = .8985$ m Ω, $R_3 = 8.828$ m Ω, $C_1 = 1.213$ μf, $C_2 = 0.1133$ μf, and $C_3 = 6.338$ μf. Some degree of optimization is available should element sizes be a critical factor.

The above circuit was initially mechanized for use in this study and operated satisfactorily. However, the necessity for fixed elements makes this circuit too inflexible for use in a simulator study, and it proved more convenient to operate on $E_i(s)$ with the elements of a partial fraction expansion of the required transfer function. The form of the required expansion is a function of τ_1 and τ_2. If τ_1 is not equal to τ_2 the expansion is:

$$\frac{E_o(s)}{E_i(s)} = \frac{K_1 g_o}{S} + \frac{K_1 g_o \tau_1^2 - \tau_1 + K_2}{(\tau_2 - \tau_1)(\tau_1 S + 1)} - \frac{K_1 g_o \tau_2^2 - \tau_2 + K_2}{(\tau_2 - \tau_1)(\tau_2 S + 1)}$$

but if τ_1 equals τ_2 the expansion is:

$$\frac{E_o(s)}{E_i(s)} = \frac{K_1 g_o}{S} - \frac{K_1 g_o \tau_1^2 - K_2}{\tau_1 (\tau_1 S + 1)} - \frac{K_1 g_o \tau_1^2 + K_2 - \tau_1}{\tau_1 (\tau_1 S + 1)^2}$$

For this study it was assumed that $\tau_1 = \tau_2 = 1$. The second form of the expanded transfer function then resulted in the following circuit:

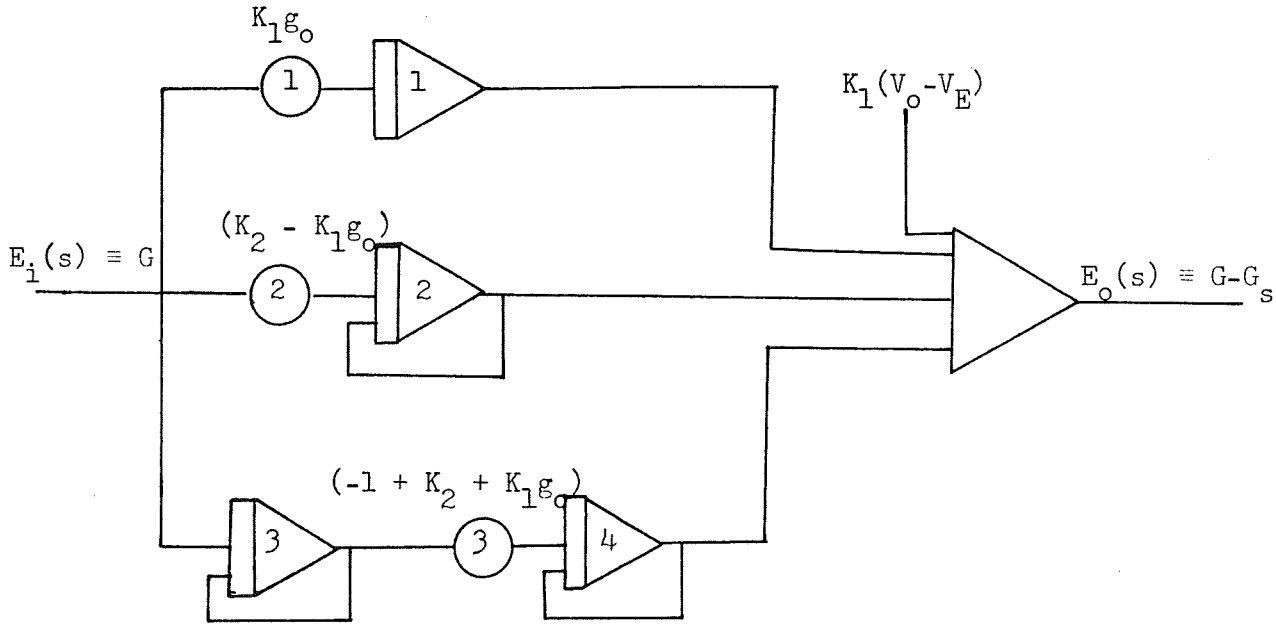

Integrator number three in this circuit can be eliminated by setting potentiometer number three to a value of

$$\frac{-1 + K_2 + K_1 g_o}{K_2 - K_1 g_o}$$

and using the output of integrator number two as the input to potentiometer number three. The advantage of the preceding circuit is that there is a direct correspondence between the gains of the components of the expanded form of the transfer function and the potentiometer settings.

Either of the circuits discussed herein will yield the quantity $G-G_s$. Remembering that the circuits actually operate on the drag acceleration rather than the total acceleration, it is technically necessary to convert the output of either circuit to account for this. In practice the conversion is not necessary since the circuit gains are set to indirectly perform the conversion internally.

APPENDIX B

It is shown in reference 4 that a suitable (but not optimum) value of L/D for a given set of flight conditions and a desired range X_T can be computed as:

$$L/D_c = K_1 + K_2 K_{\dot{h}} \left(\dot{h} + \dot{h}_b - \dot{h}_r \right) + K_3 K_A \left(a - a_r \right) + K_4 \left(K_5 - X_{rT} - X_T \right),$$

where

$$-L/D_{max} \leq L/D_c \leq L/D_{max}$$

The bank angle corresponding to L/D_c may be computed as:

$$\phi_c = \left[\cos^{-1} \frac{L/D_c}{L/D_{max}} \right] \text{SGN } Y_T$$

Range- and crossrange-to-go are, approximately:

$$X_T = R_E \left[\left(\lambda_T - \lambda \right) \sin \Psi_h + \left(L_T - L \right) \cos \Psi_h \right]$$

$$Y_T = -R_E \left[\left(L_T - L \right) \sin \Psi_h - \left(\lambda_T - \lambda \right) \cos \Psi_h \right]$$

A complete analysis of the equation for L/D_c is given in reference 4. Therein it made clear that:

1. A single reference trajectory $\left(\dot{h}_r, a_r, X_{rT} \right)$ is stored as a function of velocity V_I.

2. K_1 is a constant representing the reference L/D (herein 0.1).

3. K_2, K_3, K_4 are a set of analytically determined linear gains, stored as functions of velocity.

4. K_5 is the total range of the reference trajectory.

5. K_h and K_A are empirically determined weighting factors and are functions of velocity and initial range-to-go.

Neither the reference trajectory nor the gains and weighting factors are unique. The set used for this simulation were not necessarily optimum, but nevertheless yielded excellent results.

As with most practical entry guidance systems for use with fixed trim vehicles, crossrange is corrected with the "left-over" lift. This can lead to undesirably frequent changes in the sign of the commanded roll angle for small crossrange errors. However, it is a simple matter to inhibit the frequency of the sign changes when the crossrange errors are small compared to the vehicle's crossrange capability. An adequate approximation of the crossrange capability can be obtained by multiplying the square of velocity by a suitable constant. In the manual mode, the pilot can make a reasonable estimate of the crossrange capability with no computations required.

TABLE 1.- MASS AND INERTIA CHARACTERISTICS OF SIMULATED VEHICLE

m	264.2 slugs
I_x	3,774 slug-ft^2
I_y	3,395 slug-ft^2
I_z	3,186 slug-ft^2
I_{xz}	30 slug-ft^2
σ_x	-0.2533 ft
ϵ_z	0.7 ft

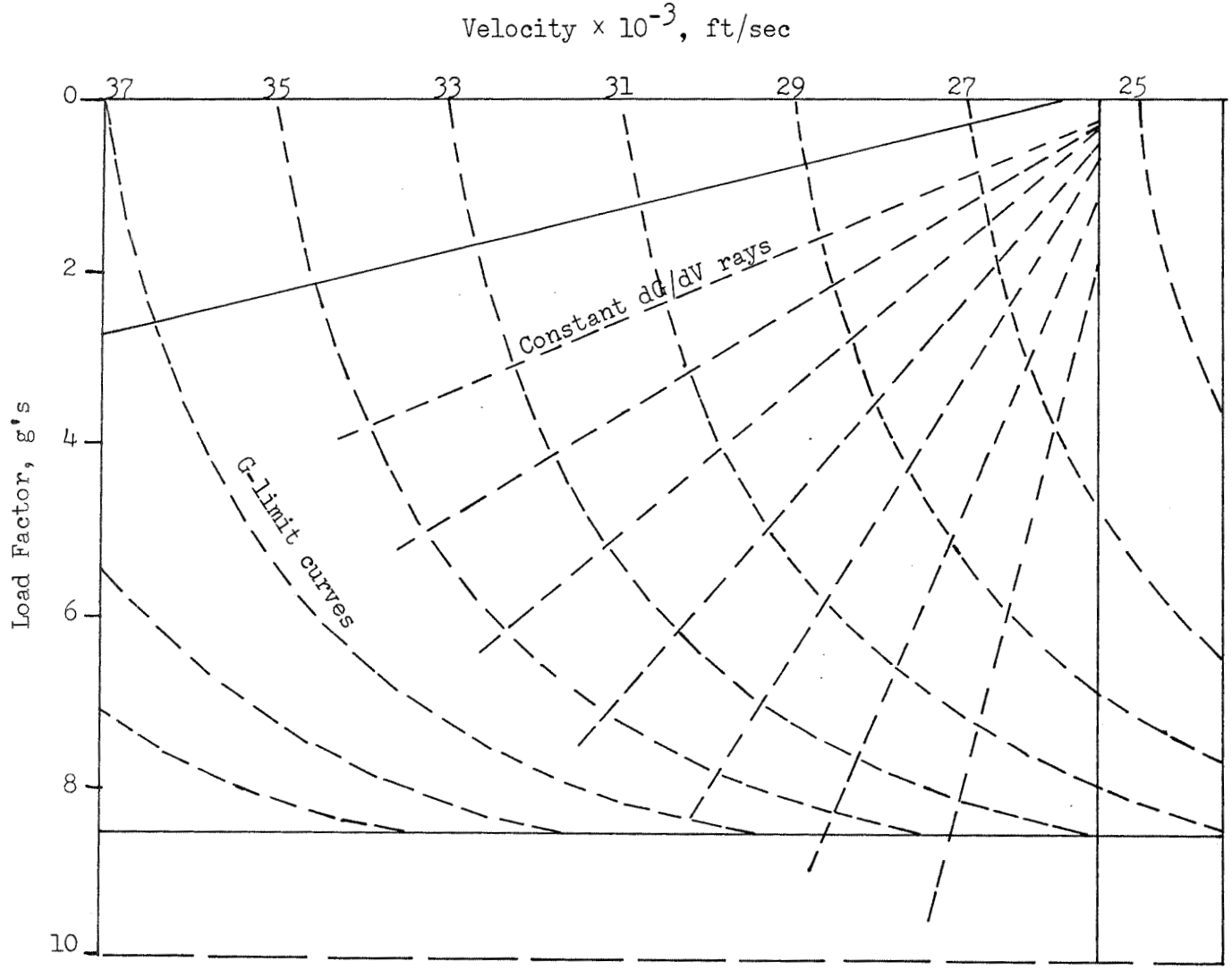

Figure 1.- Schematic of the G-V flight monitor

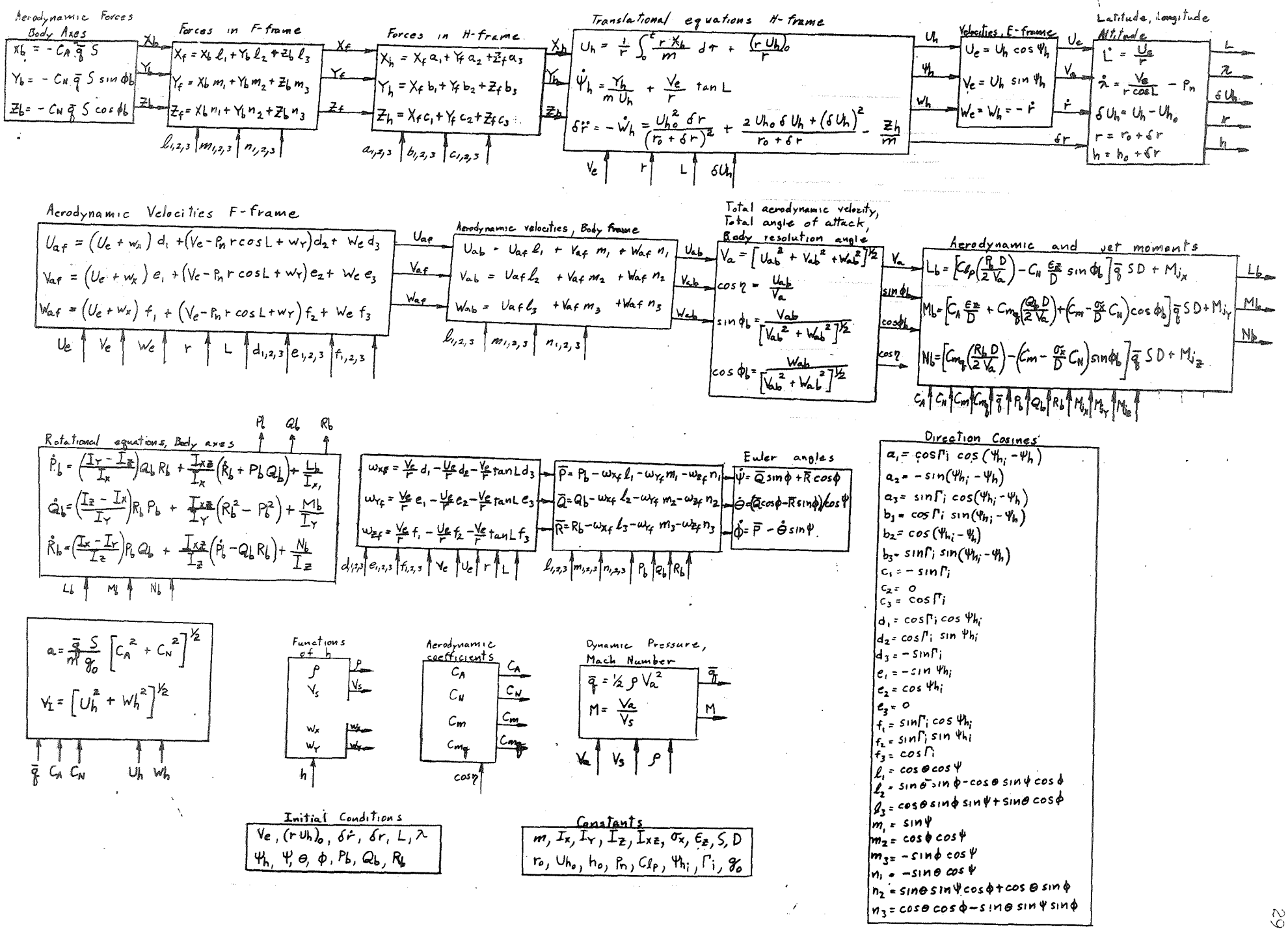

Figure 2.- Block diagram of the equations of motion

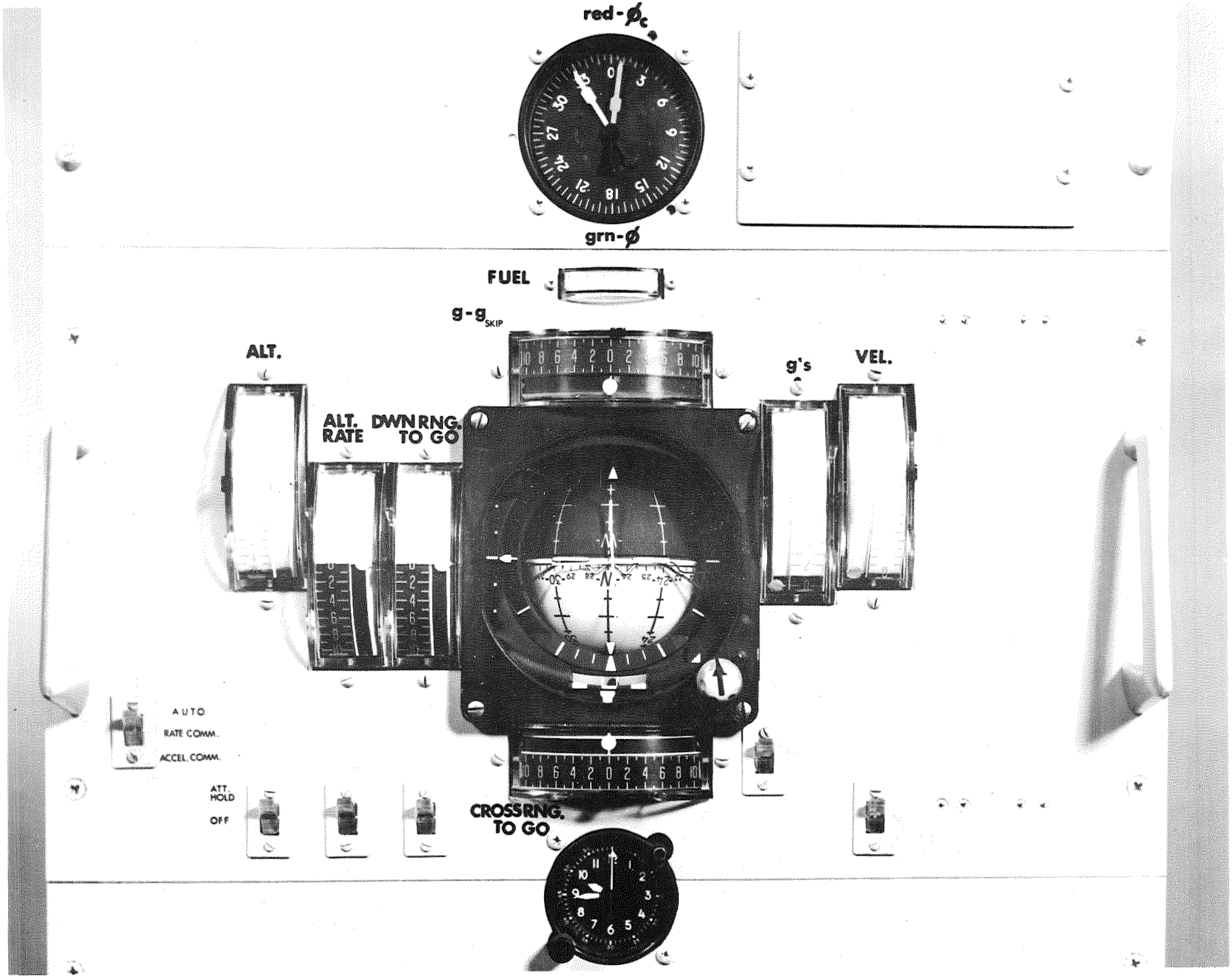

Figure 4.- Primary instrument panel

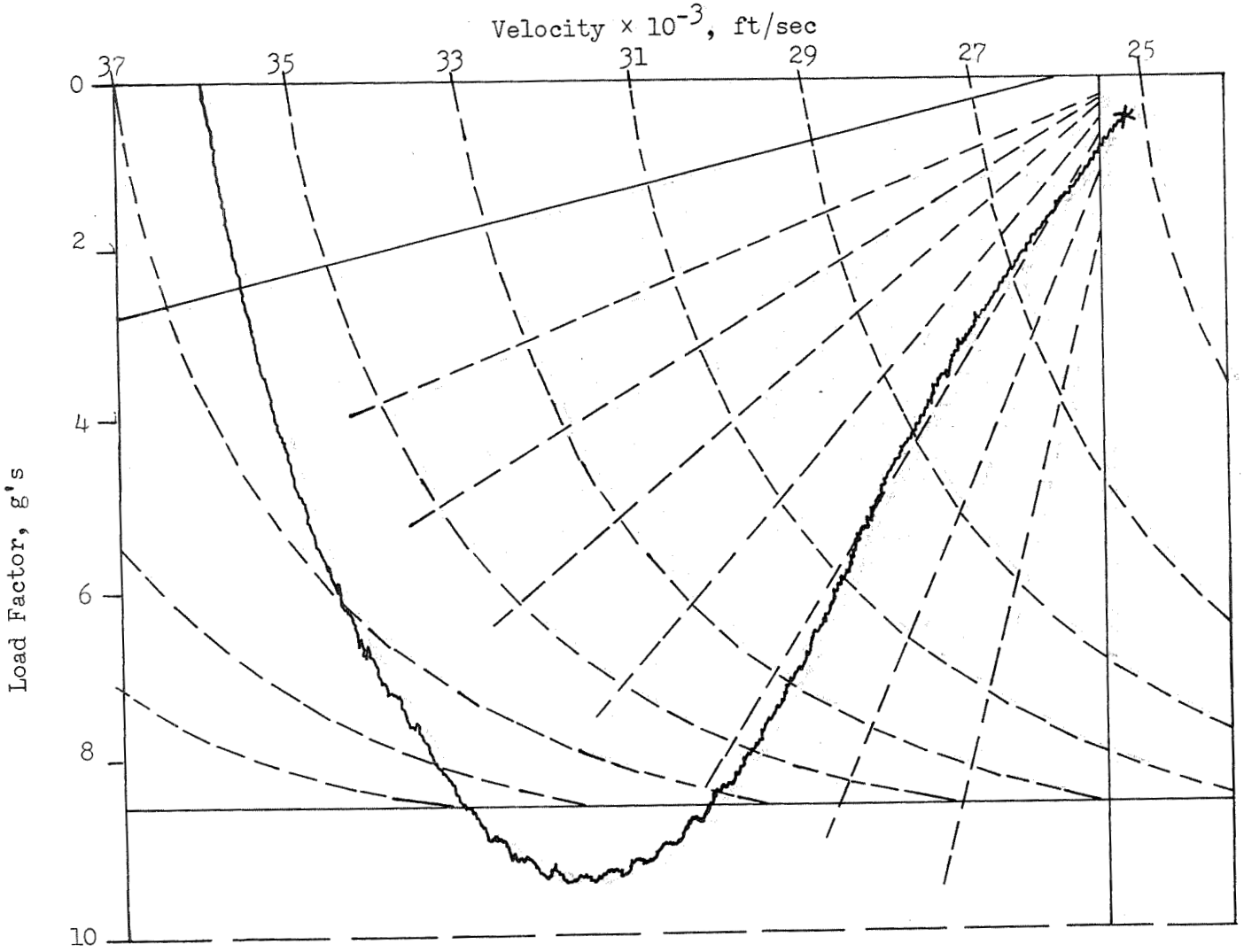

Figure 5.- G-V trace of a normal 5,000 nautical mile entry from an initial flight-path angle of -7.4°.

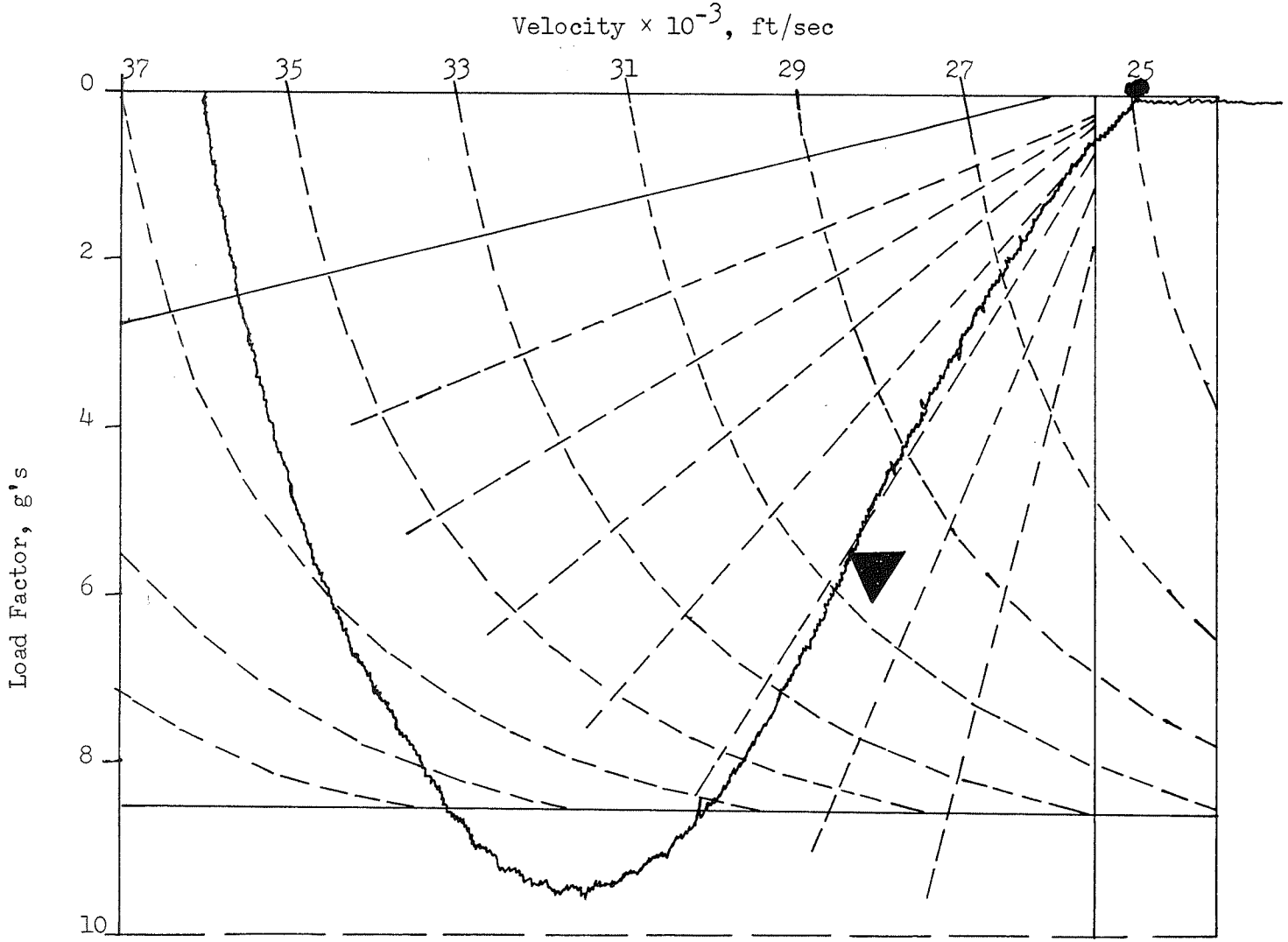

Figure 6.- G-V trace of a 5,000 nautical mile entry from an initial flight-path angle of -7.4°, with the primary guidance system failure. Pilot take-over at Δ.